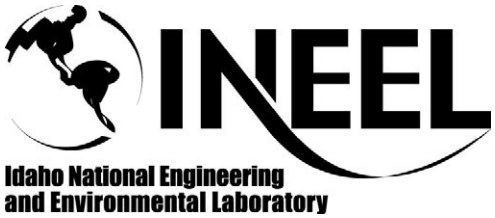

INEEL/CON-04-02353
PREPRINT

Collaborative Physical And Biological Dosimetry Studies For Neutron Capture Therapy At The RA-1 Research Reactor Facility

David W. Nigg
Amanda E. Schwint
John K. Hartwell
Elisa M. Heber
Veronica Trivillin
Jorge Castillo
Luis Wentzeis
Patrick Sloan
Charles A. Wemple

October 4-6, 2004

America's Nuclear Energy Symposium 2004

Collaborative Physical and Biological Dosimetry Studies for Neutron Capture Therapy at the RA-1 Research Reactor Facility

David W. Nigg[1], Amanda E. Schwint[2], John K. Hartwell[1], Elisa M. Heber[2], Veronica Trivillin[2], Jorge Castillo[2], Luis Wentzeis[2], Patrick Sloan[3], Charles A. Wemple[1]

1. *Idaho National Engineering and Environmental Laboratory, Idaho Falls, ID, USA.*
2. *Comisión Nacional de Energía Atómica, Centro Atómico Constituyentes, Buenos Aires, Argentina*
3. *University of Illinois, Champaign-Urbana, Illinois, USA*

ABSTRACT

Initial physical dosimetry measurements have been completed using activation spectrometry and thermoluminiscent dosimeters to characterize the BNCT irradiation facility developed at the RA-1 research reactor operated by the Argentine National Atomic Energy Commission in Buenos Aires. Some biological scoping irradiations have also been completed using a small-animal (hamster) oral mucosa tumor model.
Results indicate that the RA-1 neutron source produces useful dose rates but that some improvements in the initial configuration will be needed to optimize the spectrum for thermal-neutron BNCT research applications.

1.0 INTRODUCTION

The National Atomic Energy Commission of Argentina (CNEA) has constructed a thermal neutron source for possible use in Boron Neutron Capture Therapy (BNCT) applications at the RA-1 research reactor facility located in Buenos Aires. The Idaho National Engineering and Environmental Laboratory (INEEL) and CNEA, under a bilateral US/Argentina agreement on peaceful uses of nuclear science, have jointly conducted some basic physical dosimetric characterization measurements and some limited small-animal radiobiological dose ranging studies focused on investigation of the potential utility of this neutron source for neutron capture therapy preclinical research applications. The experimental protocol for the physical dosimetry included several sets of standard activation measurements to characterize the neutron spectrum and dose parameters at the irradiation location as well as a set of thermoluminescent dosimeter (TLD) measurements to characterize the gamma field. The radiobiological studies employed a hamster cheek pouch oral cancer model validated for BNCT studies by CNEA using an alternate, hyperthermal, neutron source available at the RA-6 research reactor in San Carlos de Bariloche, Argentina[1,2]. The work presented here has been motivated by the fact that the RA-1 facility is co-located with the CNEA radiobiological research laboratories in Buenos Aires, thereby offering some potential advantages in terms of geographical convenience, cost, and research productivity.

2.0 DESCRIPTION OF THE RA-1 FACILITY

The RA-1 reactor, with a rated operating power of 40 kilowatts, is of the open-tank type with an enriched uranium (20% ^{235}U) oxide annular core, moderated and cooled by demineralized light water and reflected internally and externally by graphite. The core is formed by 228 cylindrical fuel rods distributed in five concentric circles as shown in Figure 1. The outside diameter of the core is 335 mm and the inside diameter is 153 mm. Each fuel element is composed of a UO_2 fuel segment with an active axial length of 540 mm and 60mm graphite reflector segments on each end, with all three axial segments encapsulated in aluminum cladding with a thickness of 1 mm and an outside diameter of 10 mm.

Figure 1. View into the RA-1 tank from the top showing the annular lattice of water-moderated fuel elements.

The reactor is controlled by means of four cadmium rods encapsulated in stainless steel, located between the core and the external reflector, azimuthally separated from each other by 90 degrees. The control rods are coupled by electromagnets to drive mechanisms located in the metal structure above the tank. The drive mechanisms are powered by stepper motors operated from the control room. A set of sensors constantly transmits the exact position of each rod.

A transverse sectional view of the reactor and the adjacent graphite thermal column and shielding structure is shown in Figure 2. To produce the irradiation configuration, a cavity was made in the previous solid graphite thermal column as shown. This allowed an irradiation position closer to the reactor core, increasing the neutron flux compared to the case with the full-thickness thermal column (1600 mm) albeit at the cost of some decrease in the thermal nature of the spectrum that is produced. A small cart that moves in and out of the cavity using a system of tracks and pulleys is then used to position the experimental animals at the irradiation point. This cart is shown in Figure 3. A "shielding box" constructed from laminated plates composed of 6 mm of enriched lithium carbonate sandwiched between thin sheets of Lucite™ is mounted on hinges connected to the bed of the cart. The cart is moved into the cavity with the shielding box in the folded position. The box is then rotated upright on the hinges to position the experimental animals for irradiation.

Figure 4 shows how the experimental animals are positioned in the shielding box, which is designed for irradiation of two animals at a time. A Lucite™ hamster phantom is shown in one of the two available positions. In the case of an actual hamster, the cheek pouch, i.e. either a normal non-cancerized pouch or a tumor-bearing cancerized pouch, is everted and spread on the flat surface to the animal's right. A lithium-lucite cover plate is then placed over the hamster. The arrangement allows the cheek pouch to be exposed to essentially the full thermal flux field at the irradiation point while reducing the thermal neutron flux in the main body of the hamster via thermal neutron capture in the surrounding ^{6}Li, which captures neutrons without producing secondary gammas.

Figure 5 shows the assembled cart and shielding box positioned at the entrance to the irradiation cavity in the thermal column. Figure 6 shows a view into the cavity with the cart in the irradiation position prior to rotation of the shield box. Irradiations are conducted by first bringing the reactor to its rated power of 40 kW, sliding the cart into position to begin the irradiation, and then withdrawing it to end the irradiation after the desired time has elapsed.

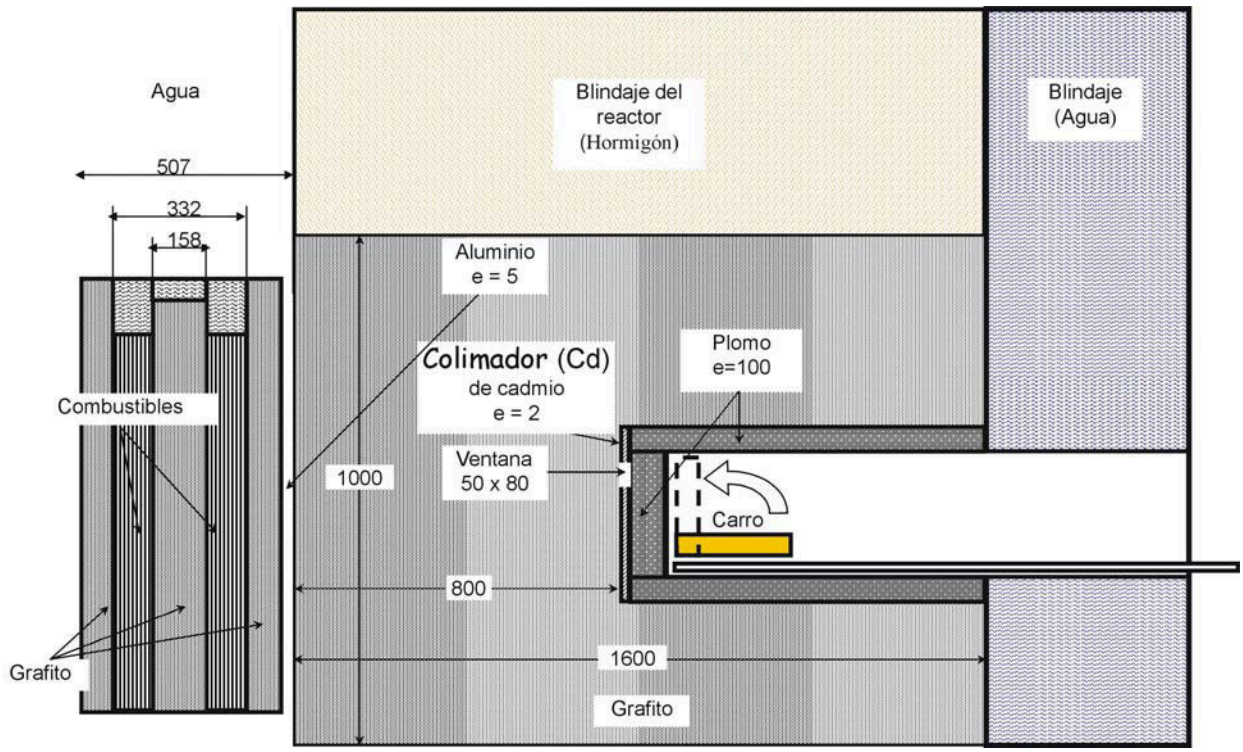

Figure 2. Transverse section of the RA-1 reactor and adjacent thermal column, taken through the core centerline. (Note: Combustibles=Fuel Elements , Blindaje = Shielding, Hormigon = Concrete, Agua =Water, Plomo = Lead, Ventana=Window, e=espesor=thickness. All dimensions are in mm).

Figure 3. Irradiation cart with lithium carbonate lined shielding box in the folded (left) and upright (right) positions.

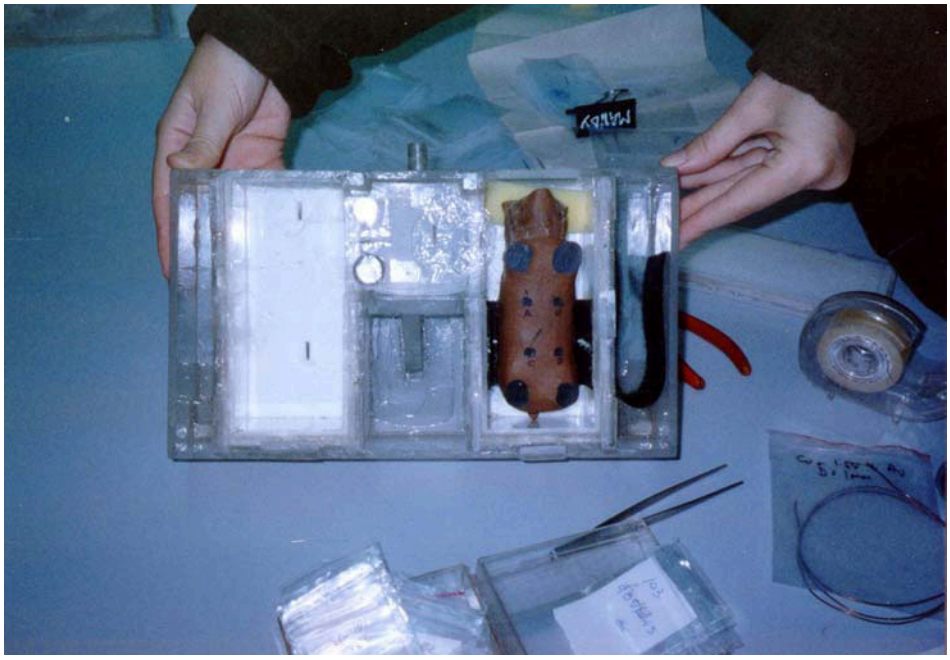

Figure 4. Shielding box with hamster phantom in position, prior to placement of lid.

Figure 5. Irradiation cart with assembled shielding box, positioned at the entry to the thermal column.

Figure 6. View into the thermal column penetration showing the irradiation cart in position at the irradiation point prior to rotation of the shield box into the upright position.

3.0 PHYSICAL DOSIMETRY

The neutron field characterization measurements were performed using simplified extensions of neutron activation analysis techniques[3,4] that have been adapted for BNCT applications by the INEEL through extensive experience with several other medical neutron facilities in the U.S. and in Europe. Gamma field measurements were conducted using standard thermoluminescent dosimeters (TLD). Auxiliary neutron transport computations of various types are also required as part of the experimental protocol. The various computational and experimental methods used for the RA-1 source characterization are described in the following sections.

A. Computational Methods

The *a-priori* spectrum produced by the RA-1 facility at the irradiation location was computed using the well-known DORT discrete-ordinates transport code[5] with the BUGLE-80 47-group neutron cross section library[6]. The reactor and thermal column arrangement shown in Figure 2 was approximately modeled in two-dimensional cylindrical geometry with the z-axis coinciding with the axis of neutron flow from the reactor, through the graphite thermalization region and into the irradiation cavity, i.e from left to right in Figure 2. This required approximating the reactor core as a cylinder on its side, but experience has shown that this approximation is appropriate provided that key region volumes, core reactivity, and key region thicknesses along the axis of neutron flow are preserved. Additional calculations to determine spectrum unfolding parameters for the activation measurements were performed using the computed flux taken from the DORT model at a transverse plane just upstream of the irradiation point, coupled with an MCNP[7] Monte Carlo transport model of the activation foil and wire packages.

B. Activation Foil Measurements in the Free Beam

Activation measurements to characterize the free-field neutron source were conducted using neutronically thick circular foils of various types. The foil specifications and corresponding neutron activation interactions of interest are listed in Table 1. Because of the limited time available, a very simple set of foils was used for these measurements. Nonetheless, useful results were still obtained.

The basic experimental arrangement for positioning the foils in the beam is shown in Figure 4. Standard 12.7-mm (0.5") diameter gold, copper, tungsten,and indium foils were placed in the irradiation position occupied by the the everted hamster cheek pouch on the outer surface of the shielding box. A cadmium cover was placed around this set of foils to suppress the thermal-neutron response. Each cadmium-covered foil thus responds largely to neutrons having energies at or near the energy of the respective primary resonance of the foil material, as shown in Table 1. Uncovered gold and manganese foils were also placed in the irradiation position to permit a measurement of the thermal flux. The foils had nominal thicknesses in the range of 0.0254 mm (0.001") to 0.127 mm (0.005"), depending on the material type.

Table 1. Activation interactions and foils used in the INEEL/CNEA measurements.

Neutron Interaction	Energy Range of Primary Response	Activation Gamma Energy of Interest (keV)
^{55}Mn (n, γ) Bare Foil	Thermal	847
^{197}Au (n, γ) Bare Foil	Thermal	411
^{115}In (n, γ) Cd Cover	1 eV Resonance	1293,1097, and 416
^{197}Au (n, γ) Cd Cover	5 eV Resonance	411
^{186}W (n, γ) Cd Cover	18 eV Resonance	686
^{63}Cu (n, γ) Cd Cover	1 keV Resonance	511 (Positron)
^{115}In (n,n') Cd Cover	430 keV Threshold	336

The cadmium covered indium foil was also used to provide additional spectral information in the energy range above epithermal (> 10 keV). In addition to the prominent gamma lines from ^{116}In that result from neutron capture in ^{115}In there is also a relatively weak 336 keV gamma line from an isomer of ^{115}In that is formed by inelastic scatter. This latter interaction can be used to gauge the neutron flux above the threshold for this interaction (~400 keV).

.

Use of the foils as described provided 7 basic neutron response functions having a useful degree of linear independence. These response functions were:

1. Resonance capture in the copper, tungsten, and gold, and indium foils, all with thermal neutron capture suppressed by cadmium (4 responses);

2. Total neutron capture in the uncovered gold and manganese foils (2 responses);

3. Inelastic scatter in the cadmium covered indium foil (1 response).

The measurements reported here are based on the results of a one-hour irradiation at a reactor power of 40 kW.

The irradiated foils were assayed using a new Ortec gamma spectrometer system recently placed into operation at the CNEA reactor laboratory. The system consisted of an HPGe detector and a a DigiDart™ digital gamma ray spectrometer, coupled with the Gamma Vision™ data acquisition and analysis software. This detector system was calibrated for energy and efficiency using standard traceable sealed gamma sources available at the CNEA laboratory. The final measured saturation activities for the foils are presented in Table 2. Some additional independent measurements of the activation of cadmium-covered gold and indium foils and for a bare gold foil were performed by the CNEA staff separately from the collaborative measurements performed by INEEL personnel. The results of these measurements, also shown in Table 2, serve to help validate the larger set of measurements performed in the collaboration with INEEL.

Table 2. Saturation activities for the foils used in the RA-1 free beam spectrum measurements. Uncertainties are given in parentheses at the 1σ level.

Interaction Type	Measured Activation Rate per Atom (INEEL)	Measured Activation Rate per Atom (CNEA)
Mn-55 (n,γ) – No Cd Cover	1.96×10^{-15} (3.0%)	
Au-197 (n,γ) – No Cd Cover	1.86×10^{-14} (3.1%)	1.96×10^{-14} (10.0%)
In-115 (n,γ) – Cd Cover	9.60×10^{-15} (3.2%)	
Au-197 (n,γ) – Cd Cover	3.85×10^{-15} (3.1%)	3.53×10^{-15} (11.3%)
W-186 (n,γ) – Cd Cover	2.15×10^{-15} (6.4%)	
Cu–63 (n,γ) – Cd Cover	3.89×10^{-17} (6.6%)	
In–115 (n,n') - Cd Cover	3.93×10^{-18} (13.5%)	3.63×10^{-18} (8.3%)

C. Phantom Measurements

Measurements of the thermal and epithermal neutron distribution at various points on the surface of and within the lucite hamster phantom were also conducted, primarily to estimate the effect of placing the hamster in the shielding box, which was designed to reduce the thermal neutron flux in the main body of the hamster relative to that seen by the everted cheek pouch on the outer surface of the box, as discussed previously. Figure 4 shows the hamster phantom in position – in an actual animal irradiation the cheek pouch would be everted to expose the tumors and extended to the hamster's right in the photo, with the tumor region placed roughly at the location of the flux wire that can be seen to the phantom's right in the photo. The flux wires used for the measurements reported here were approximately 8 mm in length and 1 mm in diameter. Each wire had a mass of approximately 70 mg and was composed of copper alloyed with 1.55 percent gold by weight. This provided two linearly-independent activation responses (neutron absorption in Cu-63 and Au-197) that were used to estimate the flux distribution in and around the hamster phantom. The activation responses of the wires could also be used to unfold a two-group (thermal and above-thermal) neutron spectrum at each flux wire location but this was not done in the work presented here. Wires were placed at the irradiation location where the everted cheek pouch would be, as well as in holes drilled at various points throughout the phantom head and body and at various locations on the hamster surface. There were 15 wires in total.

D. Spectral Unfolding Procedure

The activation rates of the various foils and wires were used to estimate the neutron spectrum of the RA-1 beam and the fluxes in the water phantom by way of a direct least-squares unfolding procedure adapted by the INEEL for this type of measurement and documented in Reference 8. For convenience, the basic derivation of the method is repeated here:

The volume-average activation rate per atom for a foil dosimeter placed in a neutron flux field may be calculated as:

$$R = \int_0^\infty \sigma_f(E)\, \Psi_f(E)\, dE \qquad (1)$$

where $\sigma_f(E)$ is the microscopic activation cross section of interest for the foil material, as a function of neutron energy and $\Psi_f(E)$ is the volume-average scalar neutron flux within the foil, again as a function of energy. Equation 1 can also be expressed as:

$$R = \int_0^\infty \sigma_f(E) \left(\frac{\Psi_f(E)}{\Psi(E)} \right) \Psi(E)\, dE = \int_0^\infty \sigma_f(E)\, P_f(E)\, \Psi(E)\, dE \qquad (2)$$

where $\Psi(E)$ is the unperturbed neutron flux that would exist at the measurement location in the absence of the foil and any surrounding spectral modification devices (Cd covers, boron sphere, etc).

It may be noted here that, as a practical matter, the function $P_f(E)$ in Equation 2 can be determined independently from $\Psi(E)$ if desired since it is simply a flux ratio. In this case $\Psi(E)$ on the far right hand side of Equation 2 can be any appropriate *a-priori* free-beam unperturbed flux estimate that is then modified by the self-shielding function $P_f(E)$.

Equation 2 may be written as a summation rather than as an integral by partitioning the range of the energy variable into a number of discrete contiguous energy groups:

$$R = \sum_{j=1}^{NG} a_j \phi_j \qquad (3)$$

where NG is the total number of energy groups,

$$a_j = \frac{\int_{EL_j}^{EH_j} \sigma_f(E)\, P_f(E)\, \Psi(E)\, dE}{\int_{EL_j}^{EH_j} \Psi(E)\, dE} \qquad (4)$$

and

$$\phi_j = \int_{EL_j}^{EH_j} \Psi(E)\, dE. \qquad (5)$$

where EL_j and EH_j are the lower and upper energy limits of energy group j.

If additional foils are placed in the beam, or if a particular foil exhibits more than one activation response then Equation 3 may be written as a system of equations:

$$R_i = \sum_{j=1}^{NG} a_{ij}\ \phi_j \qquad (6)$$

where R_i is the total activation rate for interaction i and a_{ij} is the activation constant from Equation 4 for reaction i from neutrons in energy group j. There will be a total of NF equations, where NF is the total number of activation responses available.

Effective shielded cross sections $\sigma_f(E)$ and the corresponding shielded and unshielded neutron fluxes suitable for computing the function $P_f(E)$ for this work were generated using an MCNP model of the foil packages and the immediately adjacent portion of the graphite thermal column. The neutron source for the MCNP computation was taken from the 47-group DORT computation in a plane several centimeters upstream from the foil irradiation positions. The MCNP computational model for the foil parameters consisted of a plane source, the last several centimeters of the thermal column structure upstream of the irradiation point, and the foil packages. The foil reaction rates and fluxes were tallied on the same 47-group energy structure as the source. Thus, in practical applications the functions $\sigma_f(E)$, $P_f(E)$, and $\Psi(E)$ are ordinarily not continuous functions. For the work reported here they are 47-group representations of the actual functions, discretized according to the BUGLE neutron energy structure as noted. The integrals in Equations 4 and 5 are actually summations over the fine-group structure within each broad group used for spectral unfolding.

The system of activation equations, Eq. 6, may be written in matrix form as:

$$\begin{bmatrix} a_{11} & a_{12} & a_{13} & \cdots & a_{1\,NG} \\ a_{21} & a_{22} & a_{23} & \cdots & a_{2NG} \\ a_{31} & a_{32} & a_{33} & \cdots & a_{3NG} \\ \vdots & \vdots & \vdots & & \vdots \\ \vdots & \vdots & \vdots & & \vdots \\ a_{NF1} & a_{NF2} & a_{NF3} & & a_{NF\ NG} \end{bmatrix} \begin{bmatrix} \phi_1 \\ \phi_2 \\ \phi_3 \\ \vdots \\ \phi_{NG} \end{bmatrix} = \begin{bmatrix} R_1 \\ R_2 \\ R_3 \\ \vdots \\ \vdots \\ R_{NF} \end{bmatrix} \qquad (7)$$

or, more compactly:

$$[A][\Phi] = [R] \qquad (8)$$

Equation 7 is exact, provided that the reaction rates R_i, the activation constants a_{ij} and the group fluxes, ϕ_j are all self-consistent. If measured reaction rates for each interaction R_i are substituted into Equation 7, a solution of the resulting new system of equations for "measured" fluxes corresponding to the measured reaction rates may also be obtained under certain conditions.

If NF = NG in Equation 7 then the matrix [A] is square, its inverse will ordinarily exist, and the unknown "measured" flux vector may be obtained by any standard solution method, provided that the rows of [A] are linearly-independent to a sufficient degree, as quantified by the dot product of each row with the others. In physical terms this implies that the response functions (cross sections) for the activation interactions used in the measurement must be selected such that they have different shapes as

functions of energy. It may be noted that positive fluxes are not guaranteed to result from this procedure, but if the elements of [A] are computed in a sufficiently valid, physically-realistic manner for the specific measurement configuration, and if the measured reaction rates are accurately determined, a positive solution can generally be obtained.

There are two possibilities for the situation where NF, the number of available activation response functions, is not equal to NG, the number of energy groups for which it is desired to obtain unfolded fluxes. If NF < NG the problem is underdetermined and additional information must be introduced in some manner to permit a realistic solution, as is done in the various types of adjustment techniques for spectrum estimation from activation data. (The iterative adjustment method used later in this work is one such method.) If NF > NG the problem is overdetermined and the "extra" information that is thereby available can be incorporated into the solution for the group fluxes by a linear least-squares fitting procedure as described below.

When NF > NG an approximation for the flux vector is sought such that the sum of the squares of the weighted differences between the measured reaction rates and the calculated reaction rates obtained by substituting the desired approximate solution vector into each row of Equation 7 is minimized. That is, we wish to minimize the quantity Δ,

$$\Delta = \sum_{i=1}^{NF} \frac{\delta_i^2}{u_i^2} \tag{9}$$

where u_i is the experimental uncertainty associated with reaction rate i and

$$\delta_i = \left(R_i - (a_{i1}\phi + a_{i2}\phi_2 \cdots + a_{iNG}\phi_{NG})\right). \tag{10}$$

To accomplish this, Equation 9 is differentiated successively with respect to each group flux and the result in each case is set to zero. This produces a new set of NG equations, one for each differentiation operation. Upon some additional manipulation the new set of equations has the following compact form:

$$[A]^T[V][A][\Phi] = [A]^T[V][R] \tag{11}$$

where [V] is an NF x NF diagonal matrix whose elements are the inverse squares of the measurement uncertainties for the NF reaction rates. Equation 11 can be expressed more compactly as:

$$[B][\Phi] = [S] \tag{12}$$

where the new matrix $[B] = [A]^T [V][A]$ will be of dimension NG x NG and the new vector [S] will be of length NG.

Propagation of uncertainties in the unfolding process can be analyzed using a standard approach. In general the measured reaction rates in Equation 11 will each have an associated experimental uncertainty. In addition there will be a component of variance in the unfolded fluxes associated with the nature of the least-squares process itself, since insertion of the unfolded fluxes back into the basic

balance equation (Equation 7) will not ordinarily produce calculated reaction rates that are the same as the measured reaction rates unless NF = NG, in which case the fluxes are forced by definition to produce the measured reaction rates exactly.

An estimate for the variance of the unfolded flux in group j may be expressed as:

$$s_j^2 = \sum_{i=1}^{NF} \left(\frac{\partial \phi_j}{\partial R_i} \right)^2 \left[\delta_i^2 + u_i^2 \right] \tag{13}$$

where δ_i is computed from Equation 10 and u_i is the experimental uncertainty associated with reaction rate i. It is therefore necessary to compute a matrix of derivatives of the group fluxes with respect to each reaction rate in order to evaluate the uncertainties in the unfolded fluxes from Equation 13.

To obtain the required matrix of derivatives the rows of Equation 11 are differentiated successively with respect to each reaction rate and the results are rearranged and combined to yield:

$$[B] \frac{\partial [\Phi]}{\partial R_i} = \left[\text{column i of } [A]^T [V] \right] \tag{14}$$

Equation 14 describes NF systems of NG simultaneous equations that can be solved to obtain all of the derivatives necessary to evaluate Equation 13 for the uncertainties associated with the group fluxes.

In the case where NF=NG the variance of the unfolded flux in group j may be expressed as:

$$s_j^2 = \sum_{i=1}^{NF} \left(\frac{\partial \phi_j}{\partial R_i} \right)^2 \left[u_i^2 \right] \tag{15}$$

where u_i is the experimental uncertainty associated with reaction rate i, as before, and Equation 14 now takes the form

$$[A] \frac{\partial [\Phi]}{\partial R_i} = \left[\text{column i of an } NG \; x \; NG \text{ identity matrix} \right]. \tag{16}$$

Equation 16 describes NG systems of NG simultaneous equations in NG variables that can be solved for the necessary derivatives. These are used to evaluate Equation 15.

The method outlined here has been implemented in a FORTRAN program SPECTRE, Version 5.2. This program reads self-shielded activation cross section functions $\sigma_f(E)$ and the a-priori volume-average unperturbed and perturbed fluxes, Ψ (E) and Ψ_f(E), in a user-specified fine-group structure for each activation foil interaction of interest. These, along with a user-input *a-priori* spectrum (which in the most rigorous case is the same as Ψ(E), as noted previously) are used to compute the elements of the matrix [A] for NG broad groups, each of which spans one or more specified fine groups. Solution of the various systems of equations to produce the unfolded fluxes and associated uncertainties corresponding to a user-input set of NF measured activation rates (and associated experimental uncertainties) is accomplished using standard Gauss-Seidel iterations, with linear extrapolation to accelerate convergence.

Finally, it is of interest to note that the inverse of the matrix [B] is a covariance matrix for the unfolded fluxes, based on propagation of the measurement uncertainties u_i. Accordingly the diagonal elements of $[B]^{-1}$ correspond to the components of the flux variance in each group that are attributable to propagation of the measurement uncertainties within that group.

E. Results

Table 3 shows the results for a three-group (thermal, epithermal, and fast) flux spectrum unfolded from the seven foil responses using the direct method described above. This particular three-group structure was selected for consistency with standard epithermal-neutron BNCT flux definition conventions. Three-group *a-priori* fluxes calculated by integration of the 47-group calculated *a-priori* flux spectrum over the energy ranges indicated are also shown. The unfolding procedure produces measured results that are significantly different from the *a-priori* flux. The measured fast and epithermal fluxes are considerably higher and the thermal flux is lower. The measured thermal flux is however quite consistent with independent results obtained earlier by CNEA using the gold activation rates shown in the right-hand column of Table 2 and Westcott theory for estimating the flux from the saturation activity. The significant difference between the computed and measured fluxes in Table 3 indicates that the approximate models used in this work, while adequate to estimate unfolding parameters for the initial measurements of interest here, should be updated to represent the RA-1 system in more detail prior to being used for actual dosimetry and irradiation planning.

Background neutron dose rates and boron dose rates per ppm boron-10 are also shown in Table 3. These were computed by combining the measured flux results with kerma factors for standard tissue developed from the basic kerma data provided in File 27 of the BUGLE library. About 85% of the neutron background dose is from hydrogen recoil and an additional 5% is from nitrogen capture. The remainder is from several minor components, primarily carbon and oxygen recoil. Finally, Table 3 includes the results of gamma dose measurements performed independently by CNEA using thermoluminescent dosimeters located in the everted pouch position on the shielding box.

Figure 7 shows the results of an alternate spectrum estimation procedure based on adjusting the 47-group *a-priori* neutron spectrum using an INEEL implementation of the iterative method described by Draper[9]. This adjustment method is a variation of the approach used in the well-known SAND-II code[10]. It attempts to find a spectrum that reproduces the measured foil responses as closely as possible by iteratively adjusting the *a-priori* fine group flux until a satisfactory result is obtained, as indicated by the behavior of the reduced chi-squared parameter for the fit and by the absence of further significant change in the adjusted spectrum from one iteration to the next. During each iteration through the energy groups, the adjustment factor for the flux in a given group is taken as the weighted sum of the ratios determined by dividing the measured reaction rate by the computed reaction rate for each foil response, where the calculated reaction rate for each response is computed using the flux spectrum from the previous iteration. The weight function is simply the macroscopic activation cross section for each foil in each group. Typically, only a few iterations through the energy groups are required to produce a reasonable result using this method. The *a-priori* and adjusted fluxes for the RA-1 neutron source are shown in Figure 7. Once again, the fast flux is increased considerably by the adjustment procedure, analogous to the results of the direct unfolding method. Integrals of the adjusted fluxes over the energy ranges for the three-group structure are also included in Table 3. These are reasonably consistent with the direct unfolding results although the fast flux is somewhat lower. This discrepancy is believed to be attributable to high statistical uncertainties in the fine-group *a-priori* fast-neutron flux spectrum. These uncertainties are reduced considerably when the three-group flux unfolding parameters are produced for the direct unfolding method by coalescing the fine-group fluxes. As a result, experience has shown that the direct unfolding results generally can be assumed to be more accurate if there are discrepancies of this type.

Table 3. Calculated and measured integral flux parameters for the CNEA RA-1 thermal neutron source facility at the irradiation point outside of the lithium carbonate shield box. Uncertainties are given in parentheses at the 1σ level. The reactor power is 40 kW.

	A-Priori Calculation	Direct Unfolding	Iterative Adjustment
Fast Neutron Flux 10 keV < E < 17.33 MeV (n/cm^2-sec)	3.80×10^6	4.72×10^7 (19.5%)	3.01×10^7
Epithermal Neutron Flux 0.404 eV < E < 10 keV (n/cm^2-sec)	1.36×10^7	5.28×10^7 (11.5%)	5.63×10^7
Thermal Neutron Flux E < 0.414 eV (n/cm^2-sec)	2.34×10^8	1.51×10^8 (3.7%)	1.83×10^8
Neutron Dose Rate (cGy/min)	0.569	6.97	4.47
Boron Dose Rate (cGy/min-ppm ^{10}B)	9.34×10^{-2}	6.03×10^{-2}	7.31×10^{-2}
Gamma Dose Rate CNEA TLD Measurement (cGy/min)	N/A	1.3	1.3

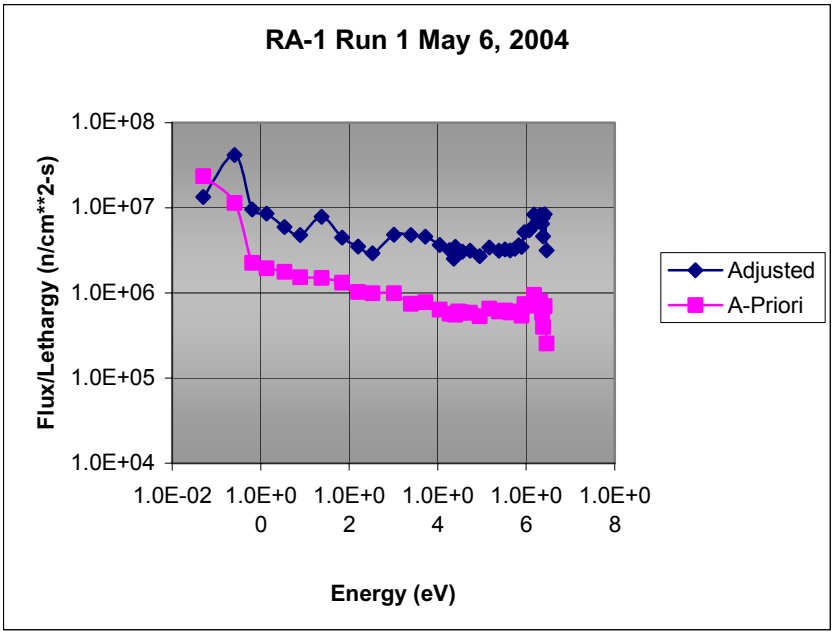

Figure 7. Unfolded free beam neutron spectrum obtained by iterative adjustment for the CNEA RA-1 thermal neutron source facility. The reactor power is 40 kW.

It is also possible to validate the directly-unfolded fast-neutron flux by further examining the activation rate of the isomeric state of ^{115}In. Recall that the inelastic scattering interaction that leads to this state, which decays with the emission of a 336 keV gamma, has a threshold in the range of 400 keV. Thus the inelastic scatter interaction rate that is measured is a direct indicator of the neutron flux above this energy. The two independent measurements of this interaction rate (Table 2) give very consistent results, roughly 3.75 x 10^{-18} interactions/atom-s, for RA-1. On the other hand, in the case of the RA-6 epithermal neutron beam in Bariloche CNEA and INEEL measured a value of approximately 1.5 x 10^{-18} interactions/atom-s for this parameter, less than half of the value measured at RA-1. Since most of the background dose in both neutron sources results from high-energy proton recoil, it follows that the background dose for RA-6 must be roughly half of that at RA-1. The RA-6 background neutron dose with the epithermal beam configuration was measured by two independent methods to be in the range of 3.4 cGy/minute. Based on this analysis one would then expect a background dose rate of roughly twice this value for RA-1, which is indeed the case, as seen in the second column of Table 3.

With regard to the phantom measurements, no fluxes were unfolded from the flux wire activation rates because of the lack of adequate computational models to compute the required parameters at this stage of the project. However, based on the copper activation rates measured for the wires it can be estimated that the thermal flux in the parts of the hamster body that are protected by the lithium shield is in the range of 20-40% of what it is at the everted pouch position, unprotected by the shield. This appears consistent with the TLD gamma measurements performed by CNEA. The gamma dose measured for the parts of the hamster body protected by the shield was generally about half of that measured for the everted pouch position. This indicates a reduction in the hydrogen capture gamma dose rate (proportional to the thermal neutron flux) in the protected regions of the phantom. The reduction is less than for the thermal flux itself because there is also a constant background gamma dose throughout the phantom inside and outside of the shield box from the incident gamma field from the reactor as well as from capture gammas in the cadmium and lead shielding in the irradiation cavity.

Using the data from Table 3, one can estimate the total physical (i.e. unweighted) dose at the irradiation location for a hypothetical, but realistic, case where there is 50 ppm in the irradiated tissue as follows:

Background Neutron Dose:	6.97 cGy/min (all sources)
Gamma Dose:	1.30 cGy/min (capture + incident)
Boron Dose:	3.02 cGy/min
Total	11.29 cGy/min

Thus the background neutron dose is over half of the total and the selective boron dose is only about 25% of the total in this case. Some improvements in the design of the RA-1 neutron source are consequently recommended to bring the relative magnitude of the boron component up into a range that is consistent with BNCT research practice elsewhere.

4.0 BIOLOGICAL DOSIMETRY

The radiobiological dose ranging studies involved two types of hamster irradiations. The first was a limited set of irradiations using the RA-1 neutron source without administration of a boron agent in order to gauge the background dose from the mixed neutron-gamma field at the irradiation location. Additionally, a few initial irradiations were performed using boronated phenylalanine (BPA) as well as a potential alternate agent for BNCT. This alternate agent, GB-10, may offer some advantages[11], either alone or in combination with the more commonly used BPA. GB-10 ($Na_2B_{10}H_{10}$) is not new, but interest in its possible use has re-emerged recently because of its biochemical performance and the development by INEEL of an improved synthesis technique for the key precursor, decaborane. GB-10 is a diffusive agent that has been shown to achieve high (~100 ppm) blood-boron concentrations in human biodistribution studies without toxicity. This is an improvement over the performance of the other largely diffusive agent that is currently approved for human studies, borocaptate sodium, or BSH. Although one

would not expect a large macroscopic tumor/blood differential to be developed with GB-10, it may be that microscopic distributions of GB-10 in and around tumor cells would be more uniform than appears to be the case with BPA. BPA, commonly used in human NCT trials worldwide, is an active agent that achieves, at least on a macroscopic scale, a significant tumor/blood differential uptake ratio, but there are questions about whether the microscopic (cell to cell) distribution is sufficiently uniform to provide adequate coverage of the target cells. Thus, if GB-10 were administered in combination with BPA one would hypothetically be trading macroscopic selectivity against microscopic uniformity in order to obtain an improved overall optimum coverage of tumor cells, so that fewer cells are left with a non-therapeutic level of boron and potentially also offering additional mechanisms for tumor control. This hypothesis has been the subject of the ongoing INEEL/CNEA collaboration using the RA-6 neutron beam and the study presented here is intended to gauge the feasibility of extending this collaboration to irradiations using the RA-1 facility.

The hamster cheek pouch oral cancer model has been validated for BNCT studies as noted previously. Successful tumor control and the absence of normal tissue radiotoxicity have been evidenced by performing *in-vivo* BNCT mediated by GB-10 and GB-10 and BPA administered jointly[1], and BNCT mediated by BPA alone[2] using the RA-6 hyperthermal neutron beam. Within this context, both normal tissue response and tumor control have been extensively characterized. Thus, we were able to assess the response of the hamster cheek pouch oral cancer model for different exposure times and irradiation conditions at RA-1 to contribute to the characterization of the this beam in terms of radiobiological parameters.

The first set of irradiations at RA-1 involved no body shielding and short (10 minutes) exposures. Six normal hamsters (non-cancerized) were irradiated with beam only, nine normal hamsters were treated with BPA-BNCT (15.5 mg ^{10}B/kg body weight) and nine normal hamsters were treated with GB-10-BNCT (50 mg ^{10}B/kg body weight). The response of normal, non-cancerized animals is clinically relevant in terms of assessing potential radiotoxicity in dose-limiting tissues in animals that will survive long enough to evidence long-term effects. Macroscopic analysis and histological evaluation revealed no radiotoxic effects up to the last experimental time-point evaluated (3 months).

Eight cancerized hamsters bearing 12 tumors were then treated with BPA-BNCT (15.5 mg ^{10}B/kg body weight) and exhibited 50% tumor control (complete remission + partial remission) by 2 weeks post-treatment associated to no radiotoxic effects. Three cancerized hamsters bearing 5 tumors were treated with GB-10-BNCT (50 mg ^{10}B/kg body weight) and exhibited 60% tumor control by 2 weeks post-treatment associated to no radiotoxic effects. These irradiations revealed that 10 minute exposures resulted in no radiotoxicity, even with whole body exposure to the beam, coupled to significant tumor control.

The second set of irradiations involved the use of the body shielding box described above as well as longer exposure times to examine the degree of protection conferred by the shielding device, the maximum tolerated exposure time and the potential tumor control associated to the varying degrees of radiotoxicity. Four normal hamsters were irradiated with beam only for 45 minutes and one normal hamster was irradiated with beam only for 60 minutes. All five hamsters have failed to evidence radiotoxic effects to date (14-76 days post-irradiation). Three normal hamsters were irradiated with beam only for 75 minutes and were sacrificed 9 days post-irradiation due to severe radiotoxicity. One normal hamster was treated with BPA-BNCT (15.5 mg ^{10}B/kg body weight) at an exposure time of 45 minutes and has failed to evidence radiotoxic effects to date (27 days post-treatment).

Two cancerized hamsters bearing 3 tumors were treated with GB-10-BNCT (50 mg ^{10}B/kg body weight) at an exposure time of 75 minutes. The animals died at 6 days post-treatment due to severe radiotoxicity and exhibited 100% tumor control. Two hamsters bearing 10 tumors were treated similarly at an exposure time of 45 minutes. The animals died 6-21 days post-treatment due to severe radiotoxicity and exhibited 90% tumor control. Two hamsters bearing 8 tumors were treated with BPA-BNCT (15.5 mg ^{10}B/kg body

weight) at an exposure time of 45 minutes. Some signs of radiotoxicity were observed coupled to 100% tumor control. One hamster bearing two tumors was treated with GB-10-BNCT (50 mg ^{10}B/kg body weight) at an exposure time of 30 minutes. To date (30 days post-treatment) it has failed to exhibit radioinduced toxicity and has evidenced 50% tumor control. One hamster bearing 8 tumors was treated with BPA-BNCT (15.5 mg ^{10}B/kg body weight) at an exposure time of 30 minutes. The animal was sacrificed at 14 days post-treatment due to moderate radiotoxicity. Tumor control was 50% for this animal.

Despite the small sample assessed, these irradiations suggest that it would not be possible to perform BNCT mediated by GB-10 or BPA alone at exposure times in excess of 30 minutes without exceeding normal tissue tolerance at RA-1. Within the context of the data obtained in previous studies at RA-6, the fact that high tumor control is associated to unacceptable radiotoxicity would suggest a proportionally small boron dose component associated to excessive background dose at RA-1. The present radiobiological findings would confirm that the background dose that would be causing the radiotoxic effects observed herein would originate in the fast neutron/gamma dose components rather than in the thermal neutron dose component for which the shielding would act as an effective protection.

The fact that BNCT mediated by the combined administration of GB-10 and BPA reduces the dose to normal tissue[1] is particularly interesting in scenarios such as RA-1 in which a reduction in background dose is particularly contributory. Within this context, and further to RA-1 optimization, studies on BNCT mediated by GB-10 + BPA are warranted within the context of escalating the dose to tumor without exceeding normal tissue tolerance.

5.0 DISCUSSION

The RA-1 facility is the second neutron source specifically constructed for NCT research in Latin America, and one of only about 12 such facilities currently operational in the world. The results presented here provide an initial assessment of the performance of this neutron source using simple but reliable experimental techniques. The results show that the neutron flux intensity is sufficient for meaningful research applications but that the spectrum is currently not optimal. However, some improvements can be made that should increase the thermal neutron flux (and thus the selective boron dose component) relative to the background fast and epithermal neutron flux and the resulting nonselective background dose.

First, it appears that the cadmium plate just upstream of the irradiation location, intended to create a narrow window for thermal neutrons and thus a local peak in the thermal flux immediately downstream may be doing more harm than good. If this plate were removed, the thermal neutron flux in the irradiation location would increase, perhaps very significantly, while the fast neutron flux would remain relatively constant. Although the thermal flux would no longer be as well localized adjacent to the everted pouch position, this may be acceptable since the hamster body is shielded by the lithium box. The use of this shielding box was not contemplated in the original design of the RA-1 irradiation facility, but now that the box is available it may be better to rely on this box rather than the cadmium plate to reduce the thermal flux in the hamster body. Removal of the cadmium would also likely reduce the incident gamma dose at the irradiation location since part of this is generated secondarily to the extremely high rate of thermal neutron capture in the plate.

Second, an advantage may be gained by some additional thickness of graphite in the upstream end of the irradiation cavity to allow more moderation of neutrons emerging from the reactor than is currently possible with the 800-mm graphite thickness of the current design. This would decrease the absolute thermal flux, because of the longer distance between the reactor and the irradiation point, but part or all of this loss may be recoverable by removal of the cadmium plate as noted above.

Finally, it would be very useful to construct some improved DORT and MCNP neutronics models of the RA-1 facility as tools for evaluating the effects of the suggested design changes noted above as well as for source optimization and irradiation planning purposes. The system models constructed as aids in these initial measurements are not of sufficient detail for design optimization, much less for planning of irradiations in radiobiological studies. Improved models could be readily constructed and would in particular be very useful in developing an optimal final design for a reconfigured RA-1 irradiation cavity.

6.0 ACKNOWLEDGEMENTS

INEEL participation in this work was sponsored by the United States Department of Energy, Office of Nuclear Nonproliferation (NN-44), through the Sister Laboratory Program at Argonne National Laboratory. The INEEL and CNEA participants would like to acknowledge the assistance and support of Dr. Basil Picologlou (ANL) Dr. Kirsten Laurin-Kovitz (ANL), Dr. Margaret Manning (DOE) and Dr. Sara Liberman (CNEA) in particular.

7.0 REFERENCES

1. V.A. Trivillin, E.M. Heber, M.A. Itoiz, D.W. Nigg, O. Calzetta, H. Blaumann, J. Longino, A.E. Schwint, “Radiobiology of BNCT Mediated by GB-10 and GB-10 + BPA in Experimental Oral Cancer”, *Applied Radiation and Isotopes*, 61:939-945, 2004.

2. E.L. Kreimann, M.E. Itoiz, J. Longhino, H. Blaumann, O. Calzetta, A.E. Schwint. Boron Neutron Capture Therapy for the Treatment of Oral Cancer in the Hamster Cheek Pouch Model. *Cancer Research (Advances in Brief)*, 61: 8638-8642, 2004.

3. D.W. Nigg, et al., “Collaborative Neutronic Performance Characterization of the FiR 1 Clinical Epithermal-Neutron Beam Facility for BNCT”, In: J.R. Venhuizen (ed,), INEEL BNCT Research Program Annual Report 1998, INEL/EXT-99-00293, April 1999, pp 13-38.

4. Y.D. Harker, et al., “Spectral Characterization of the Epithermal Neutron Beam at the Brookhaven Medical Research Reactor”, *Nuclear Science and Engineering*, 110:355-368, 1992.

5. W.A. Rhoades and R.L. Childs, "An Updated Version of the DOT-4 One- and Two - Dimensional Neutron/Photon Transport Code", ORNL-5851, Oak Ridge National Laboratory, April 1982.

6. R.W. Roussin, "BUGLE-80 Coupled 47-Neutron, 20 Gamma-Ray P3 Cross Section Library", DLC-75, Radiation Shielding Information Center, 1980.

7. Breismeister, J.F., MCNP – A General Monte Carlo N-Particle Transport Code, Version 4C, LA-13709-M, Los Alamos National Laboratory, USA, April, 2000.

8. D.W. Nigg, C.A.Wemple, R. Risler, J.K. Hartwell, Y.D. Harker, G.E. Laramore, “Modification of the University of Washington Neutron Radiotherapy Facility for Optimization of Neutron Capture Enhanced Fast-Neutron Therapy”, *Medical Physics*, **27**:359-367, 2000.

9. E.L. Draper Jr. “Integral Reaction Rate Determinations – Part I: Tailored Reactor Spectrum Preparation and Measurement”, *Nuclear Science and Engineering* **48**:22-30 (1971).

10. W.N. McElroy et al. “SAND-II Neutron Flux Spectra Determination by Multiple Foil Activation Iterative Method”, AWRL-TR-67-41, Vol 1-4 (1967).

11. E. Heber, V.A. Trivillin, D.W. Nigg, E.L. Kreimann, M.E. Itoiz, R.J. Rebagliati, D. Batistoni, A.E. Schwint, “Biodistribution of GB-10 Compound for Boron Neutron Capture Therapy (BNCT) in an Experimental Model of Oral Cancer in the Hamster Cheek Pouch, *Archives of Oral Biology* (2004) 49:313-324.